Electrochemistry

DOI: 10.1002/ange.201411544

One-Pot Synthesis of Pt–Co Alloy Nanowire Assemblies with Tunable Composition and Enhanced Electrocatalytic Properties**

Bao Yu Xia, Hao Bin Wu, Nan Li, Ya Yan, Xiong Wen (David) Lou, and Xin Wang**

Abstract: *Three-dimensional (3D) Pt-based alloy nanostructures composed of one-dimensional (1D) nanowires/nanorods have recently attracted significant interest as electrocatalysts. In this work, we report an effective solvothermal method for the direct preparation of 3D Pt–Co nanowire assemblies (NWAs) with tunable composition. The composition- and structure-dependent electrocatalytic performance is thoroughly investigated. Because of the bimetallic synergetic effect and unique structural advantage, the as-prepared 3D Pt_3Co NWA outperforms commercial Pt/carbon and Pt black catalysts and even 3D Pt NWA. The electrochemical results demonstrate that the 3D Pt_3Co NWA is indeed a promising electrocatalyst with enhanced catalytic activity and improved durability for practical electrocatalytic applications.*

Synthesis of platinum (Pt)-based nanostructures has received widespread research attention in recent years because of their high catalytic activity for many industrially important reactions.[1–3] The scarcity and high cost of Pt have directed recent research toward reducing Pt usage in these applications, but retaining or even enhancing its activity and stability.[4,5] Among these efforts, the incorporation of other metals into Pt nanostructures is one effective strategy to enhance the activity.[6–8] The improved activity is usually explained by some synergetic effects including geometric and electronic effects which originate from the lattice contraction and downshift of the d-band center of Pt in the bimetallic structures.[9] Along this direction, significant progress has been made in the controlled synthesis of Pt-based bimetallic nanocrystals with a wide range of compositions including PtPd,[10,11] PtAu,[12] PtNi,[13] PtFe,[14] PtCu,[15,16] and PtCo.[17,18] Other than composition, the morphology and structure of bimetallic Pt nanocatalysts are also generally considered critical in determining the catalytic properties.[6,16,19] Various morphologies are thus developed to improve the electrocatalytic performance.[20,21] Recent experimental results indicate that elongated one-dimensional (1D) Pt-based nanostructures in the form of nanorods,[22,23] nanowires,[24–26] or nanotubes[27] may be advantageous compared to zero-dimensional (0D) Pt nanoparticles as the former suffer less from dissolution and Ostwald ripening/aggregation.[28,29] As a result, three-dimensional (3D) Pt-based nanostructures composed of 1D nanowires/nanorods with controllable composition have emerged as a new development to further improve the activity and stability.[30–32] Besides the expected high stability, they also possess large surface area and interconnected open-pore structures which can facilitate the electron transfer and mass exchange.[16,33]

The synthesis of such 3D structures based on 1D bimetallic nanorods is not well explored yet. Nonetheless, there are some recent related reports for the formation of 3D dendritic Pt nanostructures alloyed with noble metals (e.g., Pd and Au) which are often realized by seeded growth methods.[34,35] For example, Pd-Pt dendritic nanocrystals are achieved by deposition and growth of Pt nanocrystals on Pd seeds.[36] While thermal decomposition of organometallic compounds (such as acetylacetonate and carbonyl) is often used to obtain Pt nanocrystals alloyed with transition metals (Cu,[37] Ni,[38–40] and Co[41]), those precursors are mostly very expensive and toxic. Nevertheless, one important observation is that these dendritic bimetallic nanostructures are formed by the assembly of nanoparticles and thus lead to a final structure composed of short rods or nanoparticle aggregates, which cannot maximize the structural advantages toward the improvement of electrocatalytic activity and stability.[42] To our knowledge, there is no effective synthesis method reported so far to control the bimetallic composition of 3D Pt-based nanostructures composed of nanowires. Thus, it is imperative to develop a direct approach for the synthesis of 3D Pt-based nanostructures with controllable composition that preferentially avoids the use of organometallic compound precursors.[6]

Herein, we report an effective solvothermal method for the direct preparation of 3D Pt–Co nanowire assemblies (NWAs) with tunable composition. The effects of experimental parameters on the formation of such 3D NWAs are explored in detail. More importantly, the composition- and structure-dependent electrocatalytic performance is also thoroughly investigated. Because of the bimetallic synergetic effect and unique structural advantage, the as-prepared 3D Pt_3Co NWA outperforms commercial Pt-based catalysts and even 3D Pt NWA. The electrochemical results demonstrate that the 3D Pt_3Co NWA is indeed a promising electrocatalyst with enhanced catalytic activity and improved durability for practical electrocatalytic applications.

[*] Dr. B. Y. Xia, H. B. Wu, N. Li, Y. Yan, Prof. X. W. Lou, Prof. X. Wang
School of Chemical and Biomedical Engineering
Nanyang Technological University
62 Nanyang Drive, Singapore 637459 (Singapore)
E-mail: xwlou@ntu.edu.sg
WangXin@ntu.edu.sg

[**] We acknowledge financial support from the academic research fund AcRF tier 1 (M4011020 RG8/12 and M4011253 RG 7/14), Ministry of Education, Singapore. The support by the Singapore National Research Foundation under its Campus for Research Excellence and Technological Enterprise (CREATE) programme is also acknowledged.

Supporting information for this article is available on the WWW under http://dx.doi.org/10.1002/anie.201411544.

In a typical synthesis, chloroplatinic acid solution (H_2PtCl_6, 8 wt.% solution) and cobalt chloride ($CoCl_2$) are dissolved in a mixture of heptanol ($CH_3(CH_2)_6OH$) and oleylamine (OAm) with a volume ratio of 2:8. The resultant mixture is then sonicated for 5 min to obtain a homogeneous solution (Figure S1, see Supporting Information, SI), which is then solvothermally treated in a Teflon-lined stainless steel autoclave at 170 °C for 6 h. The morphology of the obtained products is first examined by field-emission scanning electron microscopy (FESEM). As shown in Figure 1, the as-prepared

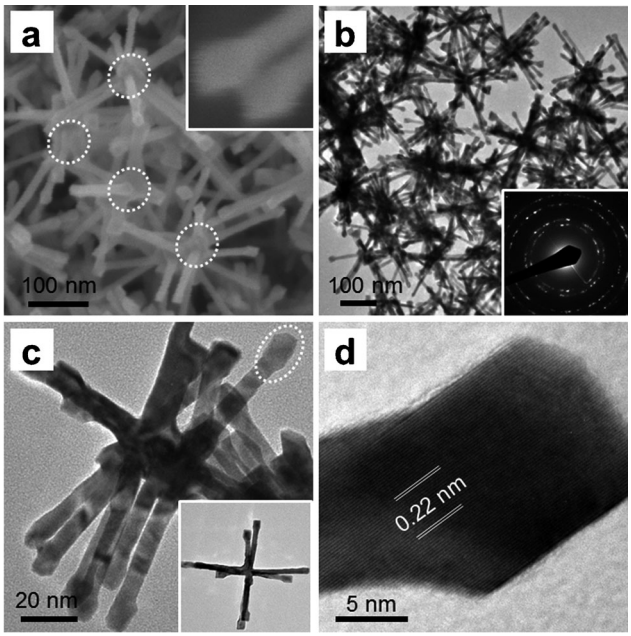

Figure 1. a) FESEM, b) and c) TEM images of 3D Pt_3Co NWA. Inset in (a) shows an enlarged image of the head of nanowires. The white circles in (a) show the center part of NWAs. The inset in (b) shows the selected-area electron diffraction (SAED) pattern. The inset in (c) shows an individual 3D Pt_3Co NWA. d) HRTEM image of the head of a nanowire indicated by a white circle in (c).

3D NWA structures are very uniform and each nanostructure is composed of many nanowires. The nanowires originate from the same center and point out in various directions to form 3D interconnected structures, as indicated by four circles in Figure 1 a. It is very interesting to observe that each nanowire branch is constructed with a stem and a cubic head, as revealed in the magnified FESEM image (inset of Figure 1 a). This feature would give a clue for the growth of nanowires which might follow an epitaxial growth mode rather than the attachment and aggregation of nanoparticles. Further insights into the morphology and structure of the 3D NWA are obtained from transmission electron microscopy (TEM) observation. Each NWA consists of 8–24 nanowire subunits (Figure 1 b,c). The diameter and length of nanowires are in the range of 5–10 nm and 100–200 nm, respectively. The selected-area electron diffraction (SAED) pattern (inset of Figure 1 b) of the NWA shows concentric rings composed of bright discrete diffraction spots, which indicates the high crystallinity. The continuous fringes run through the whole stem and head and no crystal core distortion is identified from the high-resolution (HR) TEM observation (Figure 1 d), suggesting the single-crystalline nature of each individually alloyed nanowire. Moreover, the lattice spacing of 0.22 nm is slightly smaller than that of the pure Pt (111) planes (0.23 nm), indicating the successful incorporation of Co atoms into the Pt nanostructure. Such alloyed bimetallic structures can endow Pt–Co nanocrystals with high activity and antipoisoning capability for methanol oxidation.[43]

Previously we have obtained 3D Pt NWA in OAm solution with the assistance of cetyltrimethylammonium bromide (CTAB).[44] However, it is found that the same approach cannot be extended to the synthesis of similar structures of Pt–Co alloys. In the present system, heptanol is introduced as a cosolvent/reducing agent for its high boiling point ($\approx$175 °C) and excellent intermiscibility with OAm and its presence is very important to realize the composition- and morphology-tunable synthesis of 3D Pt–Co nanostructures. Without heptanol, OAm is not able to successfully reduce Co^{2+}. Therefore, only Pt NWA is obtained (Figure S2a,b). The use of other cosolvents like ethylene glycol (EG) does not give similar 3D structures probably because of the poor intermiscibility. It is reported that hydroxy groups of heptanol are effective to facilitate supersaturation of transition metal ions and accelerate their reduction reaction.[45] Meanwhile, the presence of OAm is also critical to achieve the NWA structure. Only aggregates of nanoparticles are obtained in heptanol in the absence of OAm, although the composition agrees well with the initial precursor molar ratio (Figure S2c,d). It is believed that OAm may act as the ligand to form stable coordination complexes with Pt ions and reduce the redox potential gap.[46] The composition of Pt–Co alloys can therefore be tuned in this environment. Moreover, the volume ratio of heptanol and OAm also has significant effect on the structure of the resulting Pt–Co nanostructures (Figure S3). For example, short nanorods stand on the surface of nanoparticles with low OAm content in the mixed solvent (20 vol%). More multibranched nanocrystals are found when the volume ratio of OAm is increased to 50%. Well-defined Pt–Co NWAs are obtained when the volume ratio of OAm is increased to 80%. Previous results suggest that amine is the crucial functional group in the anisotropic formation of 1D Pt nanorods/nanowires.[47] Apparently, the interaction between OAm and different facets of Pt–Co nanocrystals plays an important role on the formation of nanowires and 3D interconnected nanostructures.

We further examine the products with different Pt/Co feeding molar ratios to understand the formation mechanism and control the composition and crystal phase. When the Pt content is dominant, as in the cases of Pt, Pt_3Co, and Pt_2Co, similar 3D nanostructures are obtained (Figure S4a–c). However, when the Pt/Co ratio is reduced to 1:1, the size of the whole nanostructure decreases to about 100 nm, whereas the diameter and length of nanowire subunits also decrease (Figure S4d). When the Pt content is further lowered, smaller dendritic nanocrystals ($\approx$50 nm) composed of nanorods ($\approx$5 nm in diameter and $\approx$20 nm in length) are formed (Figure S4e,f). Importantly, the head evolves from cubic to spherical then to octahedral on the nanorods. These results

suggest that a sufficiently high Pt content is essential for the epitaxial growth of long single-crystal Pt–Co nanowires and the eventual formation of larger 3D NWA structures with the assistance of amine groups. This understanding would be helpful for the controllable design and preparation of other Pt and transition-metal-alloyed nanostructures in the future. Also, as shown by energy-dispersive X-ray spectroscopy (EDX) (Figures S5–S10), the composition of Pt–Co products agrees well with the molar ratios of Pt/Co precursors, suggesting a complete reduction of Pt and Co precursors.

The highly crystalline and bimetallic nature of Pt–Co nanostructures is confirmed by X-ray diffraction (XRD). These diffraction peaks can be clearly indexed to face-centered cubic (*fcc*) structured Pt–Co alloys (Figure S11). When compared to pure 3D Pt NWA, the diffraction peaks gradually shift to higher 2θ values as the Co composition in the Pt–Co alloy increases (Figure 2a), which could be attributed to the decrease of lattice distance when smaller Co atoms replace Pt atoms in the lattice. Some asymmetric broadening observed in XRD patterns (Figure 2a) might be attributed to some possible microstrain existing in Pt–Co nanocrystals and the decreased particle size (Figure S4). The lattice contraction would influence the electrocatalytic properties through a possible geometric effect.[44] The composition and electronic structure of the Pt–Co bimetallic nanostructures are further investigated by X-ray photoelectron spectroscopy (XPS; Figure S12). XPS analysis of the Pt–Co bimetallic nanostructures shows a high content of metallic Pt and Co. Notably, the Pt 4f binding energy of the Pt–Co bimetallic crystals is blue-shifted compared to that of Pt. The positions of Pt $4f_{7/2}$ are 71.2, 71.4, 71.5, and 71.6 eV for Pt, Pt_3Co, PtCo, and $PtCo_3$, respectively (Figures 2b and S12b,c). It is known that the binding energy is strongly correlated with the adsorption/desorption capability of reaction species on the catalyst surface, and such a trend indicates that the d-band center of Pt–Co bimetallic nanostructures downshifts compared to that of Pt. Previous works on Pt–Co alloys also report down-shifting of the d-band center.[6,9,33] In fact, the peaks of Co 2p also blue-shift as the Co content increases (Figure S12d), implying a charge transfer from Co to Pt.

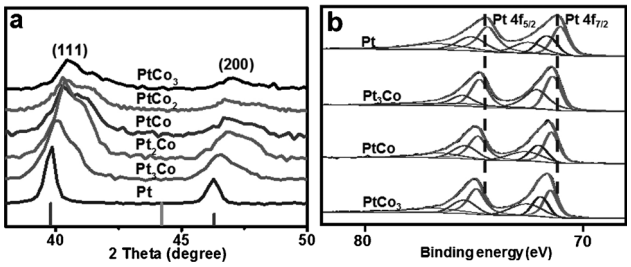

Figure 2. a) XRD patterns and b) XPS spectra of different Pt–Co NWAs.

3D bimetallic NWAs are expected to exhibit enhanced electrochemical activity. Figure 3a shows cyclic voltammograms (CVs) of 3D Pt_3Co and Pt NWAs (CVs of other Pt–Co alloys are provided in Figure S13a). The similar enhanced peak at about 0.13 V is mainly caused by the continuous step

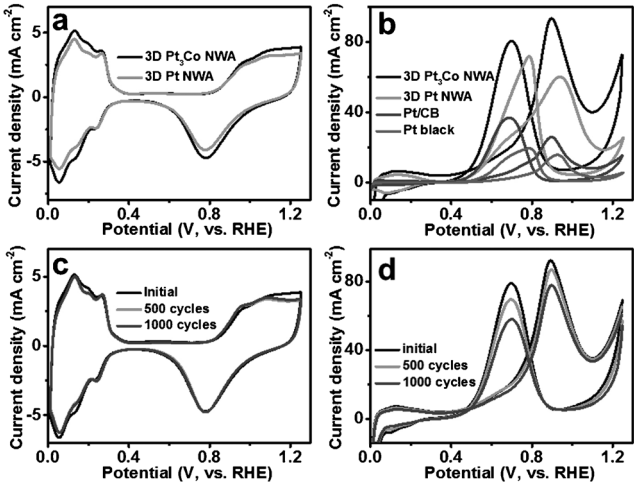

Figure 3. Cyclic voltammetry (CV) profiles of 3D Pt_3Co and Pt NWAs in 0.5 M H_2SO_4 solution (a) and in 0.5 M H_2SO_4 + 0.5 M CH_3OH solution (b). CVs of Pt/CB and Pt black are also shown in (b) for comparison. Durability tests of 3D Pt_3Co NWA in 0.5 M H_2SO_4 solution (c) and in 0.5 M H_2SO_4 + 0.5 M CH_3OH solution (d). The sweep rate is 50 $mV s^{-1}$ (RHE stands for reversible hydrogen electrode).

structure of high-index facets on the surface of nanowires. The electrochemical active surface area (ECSA) is evaluated by integrating the charge in the hydrogen adsorption/desorption region after correction for the double layer contribution. The ECSA of Pt_3Co NWA (45.2 $m^2 g^{-1}$) is slightly higher than that of 3D Pt NWA (42.9 $m^2 g^{-1}$), due to the smaller size of nanowires in the former. Figure 3b shows the CVs for methanol oxidation on Pt_3Co and Pt NWAs (CVs of other Pt–Co alloys and commercial Pt catalysts are provided in Figure S13b). The peak current density of Pt_3Co NWA is higher than that of 3D Pt NWA (94 vs. 61 mA cm^{-2}) and the peak potential is also negatively shifted by ca. 50 mV. The higher current density at lower potentials indicates an enhanced catalytic activity of the Pt_3Co NWA. This observation agrees with previous reports of Pt–Co alloyed catalysts for enhanced methanol oxidation reaction (MOR) activity. Considering that Pt and Pt_3Co catalysts have similar structures, the enhanced activity should come solely from the incorporation of Co into Pt instead of the 3D structural effect. The presence of Co may provide an oxygen source for the oxidation of CO-like intermediates at lower potentials following the bifunction mechanism.[9] Meanwhile, the electronic modification by Co introduced in Pt_3Co lowers the binding energy of Pt and favors C–H cleavage at low potential, as supported by XPS results. Electrochemical evidence of the weakened adsorption ability or lowered d-band center on the alloyed surface can be seen from the CO stripping experiment results (Figure S14), in which the peak potentials of CO stripping on all the bimetallic surfaces are lower than that on pure Pt, suggesting weaker CO adsorption strength on the former. Considering the alloying effect on the lattice contraction and electronic structure, there should exist an optimal composition,[48] and this is what is observed experimentally, where the peak potentials of CO stripping are in this particular order: PtCo (0.753 V) < Pt_3Co (0.813 V) <

$PtCo_3$ (0.843 V) < Pt (0.863 V). Moreover, we also benchmark with the electrocatalytic activities of commercial Pt black (16 mA cm^{-2} at 0.933 V) and Pt and PtRu supported on carbon black (Pt/CB, 27 mA cm^{-2} at 0.903 V; PtRu/CB, 92 mA cm^{-2} at 0.955 V) catalysts (Figure 3b, Figures S15 and S16). Clearly, both 3D Pt_3Co and Pt NWAs outperform Pt/CB and Pt black, suggesting advantages of the 3D NWA structure.[7]

We further use accelerated durability tests (ADT) as a way to characterize the short-term stability of these Pt–Co alloy catalysts in 0.5 M H_2SO_4 solution. After 1000 cycles, the ECSAs of the 3D Pt_3Co (Figure 3c) and Pt (Figure S17a) NWAs are well retained. Similarly, the stability test for the MOR is also carried out in 0.5 M H_2SO_4 + 0.5 M methanol solution. After 1000 cycles, the peak current densities of MOR are 77, 48, 8.4, 51, and 10 mA cm^{-2} for 3D Pt_3Co NWA, 3D Pt NWA, Pt/CB, PtRu/CB, and Pt black, which are about 82%, 80%, 33%, 55%, and 63% of their initial values, respectively (Figures 3d, S15, and S17). In addition, CO-stripping results also confirm that Pt_3Co and Pt NWA show an enhanced electrochemical stability compared with commercial Pt/CB and PtRu/CB catalysts (Figures S14 and S18a). Furthermore, the final current density of the 3D Pt_3Co NWA in chronoamperometric measurements is higher than those of PtRu/CB and Pt/CB, indicating that 3D Pt_3Co NWA is more active and stable than PtRu/CB and Pt/CB (Figures 4 and S18b). Much lower stability of Pt/CB and PtRu/CB is mainly caused by the severe corrosion of the carbon support in the electrochemical environment, as indicated by the decreased double layer capacitance (Figure S15a), which would result in migration and aggregation of Pt nanoparticles.[49] However, unsupported Pt black and 3D Pt–Co NWA structures do not suffer from the corrosion of amorphous carbon supports. Despite the possible Co leaching into acidic solution,[50–52] the surface atomic rearrangement in the cyclic electrochemical test would form a stable Pt-skin structure and the bifunctional mechanism would play a minimal role thereafter.[53–55] After the ADT test, XPS peak positions of Pt_3Co NWA are 71.4 eV for Pt $4f_{7/2}$ and 778.2 eV for Co $2p_{3/2}$, which are close to the initial ones (71.4 and 778.1 eV, respectively; Figures S12 and S19). It suggests that the electronic structure of the surface Pt-skin is still affected by the underneath Co atoms, thus the electronic effect is mainly responsible for the enhanced catalytic activity. The remarkable stability of 3D Pt_3Co and Pt NWAs could be ascribed to the advantage of 3D robust structure and high crystallinity, as indicated by the unchanged morphologies of 3D Pt_3Co and Pt NWAs after the ADT tests (Figure S20).

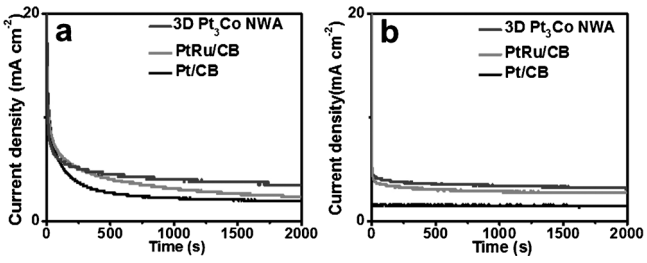

Figure 4. Chronoamperometric curves of 3D Pt_3Co NWA, PtRu/CB, and Pt/CB electrocatalysts in 0.5 M H_2SO_4 + 0.5 M CH_3OH solution recorded at 0.5 V (a) and 0.3 V (b) versus RHE.

In summary, 3D Pt–Co nanowire assemblies (NWAs) are successfully synthesized with controllable composition and morphology by a facile solvothermal method. The introduction of heptanol is critical for controlling the composition of bimetallic Pt–Co nanocrystals, and the interaction between amine groups and the Pt precursor determines the final morphology of bimetallic 3D Pt–Co nanocrystals. This understanding would be helpful for a controllable design and preparation of other Pt-based nanostructures in the future. The interconnected 3D Pt_3Co NWA exhibits significantly enhanced electrocatalytic activity and durability compared with commercial Pt based catalysts, which is mainly attributed to the synergetic effects originating from the alloyed composition and unique NWA structure.

Received: November 30, 2014
Revised: December 19, 2014
Published online: February 4, 2015

Keywords: alloys · electrocatalysis · nanostructures · platinum

[1] R. F. Service, *Science* **2002**, *296*, 1222 – 1224.
[2] V. R. Stamenkovic, B. S. Mun, M. Arenz, K. J. J. Mayrhofer, C. A. Lucas, G. Wang, P. N. Ross, N. M. Markovic, *Nat. Mater.* **2007**, *6*, 241 – 247.
[3] J. Wu, H. Yang, *Acc. Chem. Res.* **2013**, *46*, 1848 – 1857.
[4] N. S. Porter, H. Wu, Z. Quan, J. Fang, *Acc. Chem. Res.* **2013**, *46*, 1867 – 1877.
[5] Y. Wu, D. Wang, Y. Li, *Chem. Soc. Rev.* **2014**, *43*, 2112 – 2124.
[6] D. Wang, Y. Li, *Adv. Mater.* **2011**, *23*, 1044 – 1060.
[7] X. Zhao, M. Yin, L. Ma, L. Liang, C. Liu, J. Liao, T. Lu, W. Xing, *Energy Environ. Sci.* **2011**, *4*, 2736 – 2753.
[8] H. You, S. Yang, B. Ding, H. Yang, *Chem. Soc. Rev.* **2013**, *42*, 2880 – 2904.
[9] H. Yang, J. Zhang, K. Sun, S. Zou, J. Fang, *Angew. Chem. Int. Ed.* **2010**, *49*, 6848 – 6851; *Angew. Chem.* **2010**, *122*, 7000 – 7003.
[10] L. Wang, Y. Nemoto, Y. Yamauchi, *J. Am. Chem. Soc.* **2011**, *133*, 9674 – 9677.
[11] H.-H. Li, S. Zhao, M. Gong, C.-H. Cui, D. He, H.-W. Liang, L. Wu, S.-H. Yu, *Angew. Chem. Int. Ed.* **2013**, *52*, 7472 – 7476; *Angew. Chem.* **2013**, *125*, 7620 – 7624.
[12] S. Zhang, Y. Shao, G. Yin, Y. Lin, *Angew. Chem. Int. Ed.* **2010**, *49*, 2211 – 2214; *Angew. Chem.* **2010**, *122*, 2257 – 2260.
[13] V. R. Stamenkovic, B. Fowler, B. S. Mun, G. Wang, P. N. Ross, C. A. Lucas, N. M. Marković, *Science* **2007**, *315*, 493 – 497.
[14] C. Wang, Y. Hou, J. Kim, S. Sun, *Angew. Chem. Int. Ed.* **2007**, *46*, 6333 – 6335; *Angew. Chem.* **2007**, *119*, 6449 – 6451.
[15] D. Xu, Z. Liu, H. Yang, Q. Liu, J. Zhang, J. Fang, S. Zou, K. Sun, *Angew. Chem. Int. Ed.* **2009**, *48*, 4217 – 4221; *Angew. Chem.* **2009**, *121*, 4281 – 4285.
[16] X. Liu, D. Wang, Y. Li, *Nano Today* **2012**, *7*, 448 – 466.
[17] H.-P. Liang, H.-M. Zhang, J.-S. Hu, Y.-G. Guo, L.-J. Wan, C.-L. Bai, *Angew. Chem. Int. Ed.* **2004**, *43*, 1540 – 1543; *Angew. Chem.* **2004**, *116*, 1566 – 1569.
[18] C. Song, Y. Wang, N. L. Rosi, *Angew. Chem. Int. Ed.* **2013**, *52*, 3993 – 3995; *Angew. Chem.* **2013**, *125*, 4085 – 4087.
[19] J. Gu, Y.-W. Zhang, F. Tao, *Chem. Soc. Rev.* **2012**, *41*, 8050 – 8065.
[20] C. Xu, L. Wang, R. Wang, K. Wang, Y. Zhang, F. Tian, Y. Ding, *Adv. Mater.* **2009**, *21*, 2165 – 2169.

[21] B. Lim, T. Yu, Y. Xia, *Angew. Chem. Int. Ed.* **2010**, *49*, 9819 – 9820; *Angew. Chem.* **2010**, *122*, 10013 – 10014.
[22] S. Maksimuk, S. Yang, Z. Peng, H. Yang, *J. Am. Chem. Soc.* **2007**, *129*, 8684 – 8685.
[23] Q. Liu, Z. Yan, N. L. Henderson, J. C. Bauer, D. W. Goodman, J. D. Batteas, R. E. Schaak, *J. Am. Chem. Soc.* **2009**, *131*, 5720 – 5721.
[24] S. Guo, D. Li, H. Zhu, S. Zhang, N. M. Markovic, V. R. Stamenkovic, S. Sun, *Angew. Chem. Int. Ed.* **2013**, *52*, 3465 – 3468; *Angew. Chem.* **2013**, *125*, 3549 – 3552.
[25] L. Ruan, E. Zhu, Y. Chen, Z. Lin, X. Huang, X. Duan, Y. Huang, *Angew. Chem. Int. Ed.* **2013**, *52*, 12577 – 12581; *Angew. Chem.* **2013**, *125*, 12809 – 12813.
[26] H.-W. Liang, X. Cao, F. Zhou, C.-H. Cui, W.-J. Zhang, S.-H. Yu, *Adv. Mater.* **2011**, *23*, 1467 – 1471.
[27] Z. Chen, M. Waje, W. Li, Y. Yan, *Angew. Chem. Int. Ed.* **2007**, *46*, 4060 – 4063; *Angew. Chem.* **2007**, *119*, 4138 – 4141.
[28] C. Koenigsmann, S. S. Wong, *Energy Environ. Sci.* **2011**, *4*, 1161 – 1176.
[29] D. Kong, J. J. Cha, H. Wang, H. R. Lee, Y. Cui, *Energy Environ. Sci.* **2013**, *6*, 3553 – 3558.
[30] S. Sun, G. Zhang, D. Geng, Y. Chen, R. Li, M. Cai, X. Sun, *Angew. Chem. Int. Ed.* **2011**, *50*, 422 – 426; *Angew. Chem.* **2011**, *123*, 442 – 446.
[31] B. Y. Xia, H. B. Wu, Y. Yan, X. W. Lou, X. Wang, *J. Am. Chem. Soc.* **2013**, *135*, 9480 – 9485.
[32] Z. Yan, G. He, P. K. Shen, Z. Luo, J. Xie, M. Chen, *J. Mater. Chem. A* **2014**, *2*, 4014 – 4022.
[33] M. Cao, D. Wu, R. Cao, *ChemCatChem* **2014**, *6*, 26 – 45.
[34] Z. Peng, H. Yang, *J. Am. Chem. Soc.* **2009**, *131*, 7542 – 7543.
[35] B. Lim, Y. Xia, *Angew. Chem. Int. Ed.* **2011**, *50*, 76 – 85; *Angew. Chem.* **2011**, *123*, 78 – 87.
[36] B. Lim, M. Jiang, P. H. C. Camargo, E. C. Cho, J. Tao, X. Lu, Y. Zhu, Y. Xia, *Science* **2009**, *324*, 1302 – 1305.
[37] E. Taylor, S. Chen, J. Tao, L. Wu, Y. Zhu, J. Chen, *ChemSusChem* **2013**, *6*, 1863 – 1867.
[38] W. Wang, D. Wang, X. Liu, Q. Peng, Y. Li, *Chem. Commun.* **2013**, *49*, 2903 – 2905.
[39] X.-J. Liu, C.-H. Cui, M. Gong, H.-H. Li, Y. Xue, F.-J. Fan, S.-H. Yu, *Chem. Commun.* **2013**, *49*, 8704 – 8706.
[40] X. Huang, E. Zhu, Y. Chen, Y. Li, C.-Y. Chiu, Y. Xu, Z. Lin, X. Duan, Y. Huang, *Adv. Mater.* **2013**, *25*, 2974 – 2979.
[41] V. Tzitzios, D. Niarchos, M. Gjoka, N. Boukos, D. Petridis, *J. Am. Chem. Soc.* **2005**, *127*, 13756 – 13757.
[42] Z. Niu, D. Wang, R. Yu, Q. Peng, Y. Li, *Chem. Sci.* **2012**, *3*, 1925 – 1929.
[43] J. Wu, P. Li, Y.-T. Pan, S. Warren, X. Yin, H. Yang, *Chem. Soc. Rev.* **2012**, *41*, 8066 – 8074.
[44] B. Y. Xia, W. T. Ng, H. B. Wu, X. Wang, X. W. Lou, *Angew. Chem. Int. Ed.* **2012**, *51*, 7213 – 7216; *Angew. Chem.* **2012**, *124*, 7325 – 7328.
[45] D. Kodama, K. Shinoda, K. Sato, Y. Konno, R. J. Joseyphus, K. Motomiya, H. Takahashi, T. Matsumoto, Y. Sato, K. Tohji, B. Jeyadevan, *Adv. Mater.* **2006**, *18*, 3154 – 3159.
[46] S. Mourdikoudis, L. M. Liz-Marzán, *Chem. Mater.* **2013**, *25*, 1465 – 1476.
[47] Y. Wang, H. Yang, *J. Am. Chem. Soc.* **2005**, *127*, 5316 – 5317.
[48] D. Xu, S. Bliznakov, Z. Liu, J. Fang, N. Dimitrov, *Angew. Chem. Int. Ed.* **2010**, *49*, 1282 – 1285; *Angew. Chem.* **2010**, *122*, 1304 – 1307.
[49] E. Antolini, J. Perez, *J. Mater. Sci.* **2011**, *46*, 4435 – 4457.
[50] M. Pourbaix, *Atlas of Electrochemical Equilibria in Aqueous Solutions*, National Association of Corrosion Engineers, Houston, **1974**.
[51] F. Maillard, L. Dubau, J. Durst, M. Chatenet, J. André, E. Rossinot, *Electrochem. Commun.* **2010**, *12*, 1161 – 1164.
[52] M. Lopez-Haro, L. Dubau, L. Guétaz, P. Bayle-Guillemaud, M. Chatenet, J. André, N. Caqué, E. Rossinot, F. Maillard, *Appl. Catal. B* **2014**, *152 – 153*, 300 – 308.
[53] V. R. Stamenkovic, B. S. Mun, K. J. J. Mayrhofer, P. N. Ross, N. M. Markovic, *J. Am. Chem. Soc.* **2006**, *128*, 8813 – 8819.
[54] C. Wang, M. Chi, D. Li, D. Strmcnik, D. van der Vliet, G. Wang, V. Komanicky, K.-C. Chang, A. P. Paulikas, D. Tripkovic, J. Pearson, K. L. More, N. M. Markovic, V. R. Stamenkovic, *J. Am. Chem. Soc.* **2011**, *133*, 14396 – 14403.
[55] J. Durst, M. Lopez-Haro, L. Dubau, M. Chatenet, Y. Soldo-Olivier, L. Guétaz, P. Bayle-Guillemaud, F. Maillard, *J. Phys. Chem. Lett.* **2014**, *5*, 434 – 439.

